Just a little resPEPT:

An Investigation into Radial Segregation of Bidisperse Granular Media in a Rotating Cylinder

PHY3004W*

October 2017

Abstract

In this report we use positron emission particle tracking (PEPT) to study the flow of a bidisperse granular medium composed of particles of two different sizes inside a horizontal rotating cylinder. We observe that radial segregation occurs and this can be contributed to some difference in the behaviour of the particles as they flow through the free surface.

Under the supervision of Dr. Tom Leadbeater
University of Cape Town
October 2017

*Jordan Barkai, Ulrich Beckering Vinckers, Kelebogile Bonokwane, Matthew Boynton, Ihsaan Dawray, Simon De Wet, Claudia Grindlay, Rebecca Houliston, Nicholas Hyslop, Petro Janse Van Rensburg, Storm Johnson, Hanneke Le Roux, Jordan Levin, Matthew Maddock, Nkosinathi Masetlwa, Geoff Murphy, Blessed Arthur Ngwenya, Lilitha Potye, Shilpa Ranchod, Chloé Sole, Robin Visser.

Contents

1 Theory

Mixing particulate of different sizes inside a horizontal rotating cylinder is ubiquitous in industrial processing. It is known from experiment that small differences in particle size results in segregation, where particles of different sizes separate into different regions within a rotating drum, affecting the statistics of the flow of material. Segregation is unavoidable in practice and understanding this behaviour may improve the efficiency of industrial processes.

The dynamics of granular media is a challenging problem to understand as the fundamental physics of granular flow are not yet fully established, and segregation has no analogue in fluid mechanics. One would hope to have a relatively simple mathematical model for granular systems that is able to incorporate the complexities of these systems, and yet is still amenable to analysis. The most obvious way for obtaining such a method is by approximating granular materials as continua, akin to fluids. According to [3], this technique does indeed see use, but is nevertheless limiting for a number of reasons. They cite the analogy between fluids and highly heterogeneous granular systems being imperfect: certain phenomena that require the consideration of the particle nature of granular systems, such as the formation of force chains, cannot be adequately modelled using fluid-dynamical techniques. An attempt to model the flow of bidisperse granular media in a horizontal rotating cylinder is provided in Appendix A.

We consider a rotating cylinder. At low rotational speeds the flow exhibits periodic avalanches, each ending before the next begins. At high rotational speeds we observe the media cling to the surface of the cylinder. In this report we will consider the dynamics at intermediate rotational speeds where we observe a continuous flow of the medium. In the continuous flow regime, we observe a thin cascading layer, which we refer to as the free surface, which flows like a fluid. The rest of the medium, which we refer to as the bed, rotates like a solid body as shown in Fig. 1.

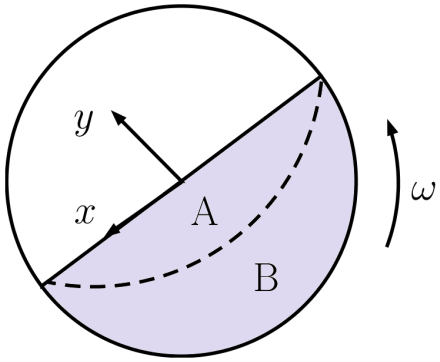

Figure 1: A schematic cross-section of the flow of granular media in a rotating cylinder. A is the free surface, which flows like a fluid. B is the bed which rotates like a solid body. ω is the angular velocity or rotational speed of the cylinder.

The Brazil nut effect describes the segregation observed when agitating a mixture of small and large particles. It is suggested that this is the result of a percolation mechanism whereby small particles fill small voids below large particles leading to irreversible segregation of smaller and larger particles. A result of the Brazil nut effect in the flowing layer of granular media in a rotating drum is size dependent radial segregation. At low rotational speeds smaller particles tend to occupy lower levels in the flowing layer which results in the formation of a "core" of smaller particles in the drum [7]. Many recent studies of radial segregation have investigated this regime. Discrete element method simulations for a two dimensional systems in the continuous flow regime was reported in [5], where it was found that the smaller particles indeed form a central core and it was suggested that this is due to the aforementioned percolation mechanism. An experimental analysis of size segregation in the continuous flow regime was reported in [2] with similar results. At higher rotational speeds in the continuous flow regime the opposite is observed; a core of the larger particles formed [7]. This behaviour is not well understood and will be explored in this report.

The use of non-invasive techniques to study granular systems is not unprecedented, [1] used magnetic resonance imaging to study the dynamics of mustard seeds in a horizontal rotating cylinder. In this analysis we will use positron emission particle tracking (PEPT) to study the dynamics and segregation of a bidisperse mixture of glass particles. We hypothesise that segregation can be attributed to different behaviour of the particles of different sizes when flowing through the free surface. This will be confirmed by illustrating that there is a difference between the velocities of the particles of different sizes as the flow through the free surface. In particular we will measure and compare the velocities in the y direction, as shown in Fig. 1, normal to the free surface.

2 Computational Simulation

In order to simulate the physics of a rotating cylinder, LAMMPS (Large-scale Atomic/Molecular Massively Parallel Simulator) [6], an open-source classical molecular dynamics simulator, was used. We utilised a set-up commonly employed for granular material simulations, described in Appendix B.

Using this set-up, we then simulated a rotating cylinder, with varying angular frequencies and varying particle number. Using a slow rotation speed and a small cylinder size, we obtain the simulation shown in Fig. 2. We note the particles stay in a single cluster throughout the simulation. This allows for axial segregation to be observed at later times in the simulation.

Finally, using a larger cylinder with many more particles, we obtain the simulation shown in Figure 3. Here, we observe a clear axial segregation after around $t = 10$ seconds.

Further results can be obtained using a higher particle number with a large cylinder, so as to ensure roughly half the cylinder is filled with particles. With these simulations, one needs to balance the CPU time required with a reasonable number of particles to ensure the simulations finish in a feasible length of time.

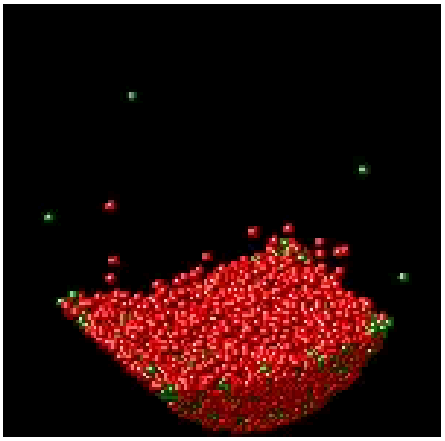

(a) Initial condition

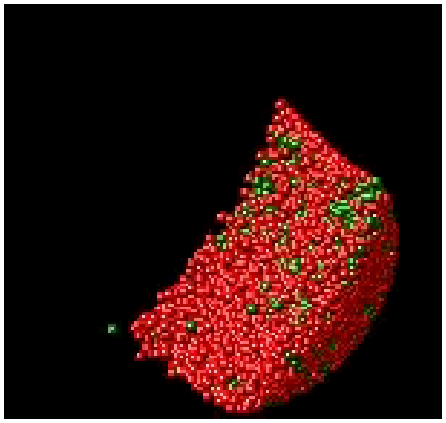

(b) System at $t = 1$ seconds

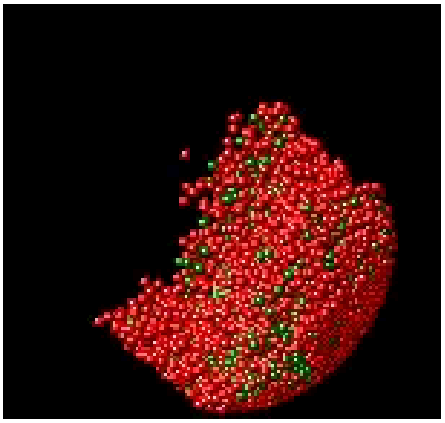

(c) System at $t = 3$ seconds

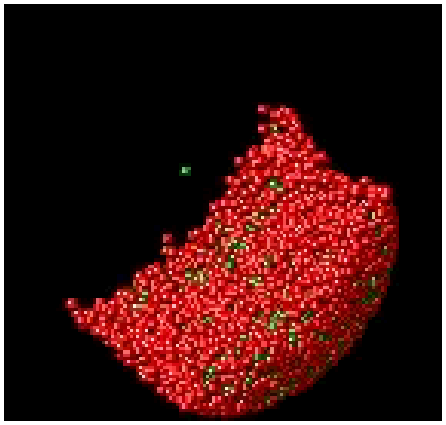

(d) System at $t = 5$ seconds

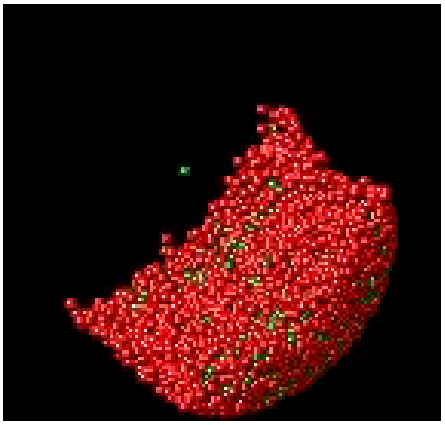

(e) System at $t = 10$ seconds

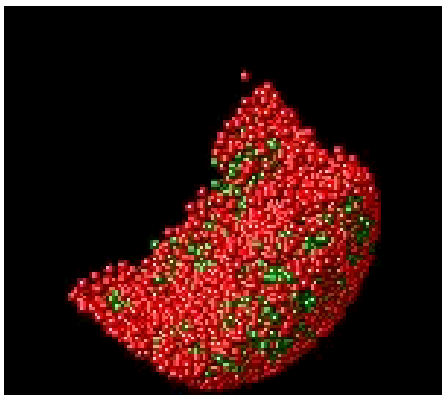

(f) System at $t = 15$ seconds

Figure 2: Simulation of particles inside a rotating cylinder at various points in time. The cylinder is rotating at 15 rotations per minute. The green particles have diameter 1.5 times that of the red particles. 10 000 of each type of particle was used. The cylinder length was 50 mm and the radius was 30 mm, with the red particle radius being 2 mm.

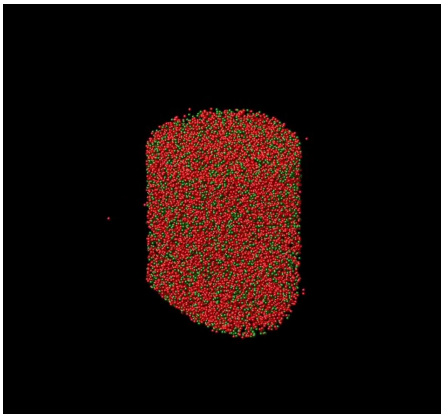

(a) Initial condition

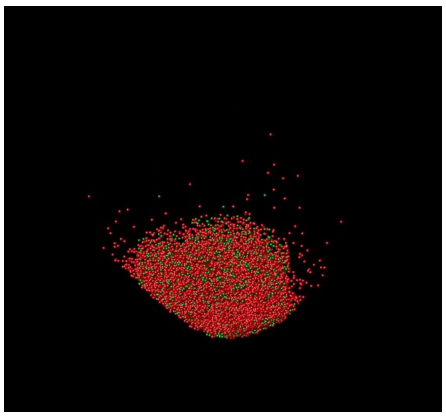

(b) System at $t = 1$ seconds

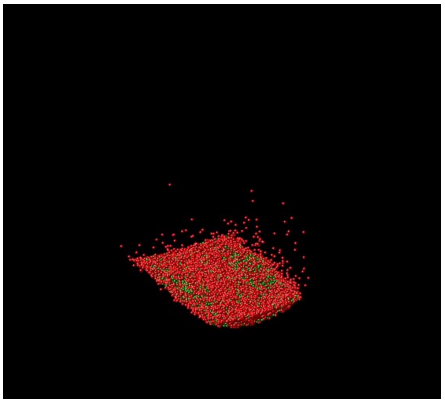

(c) System at $t = 3$ seconds

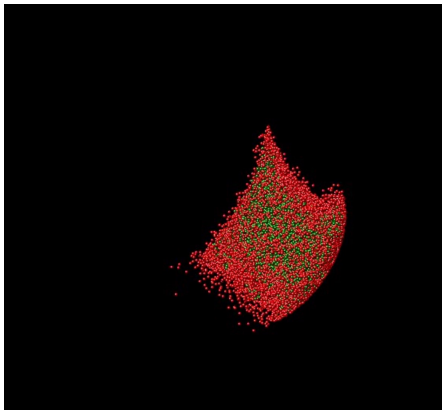

(d) System at $t = 5$ seconds

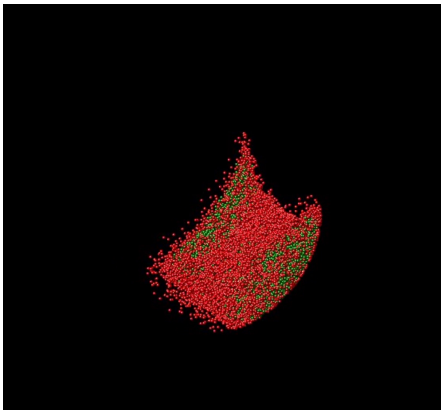

(e) System at $t = 10$ seconds

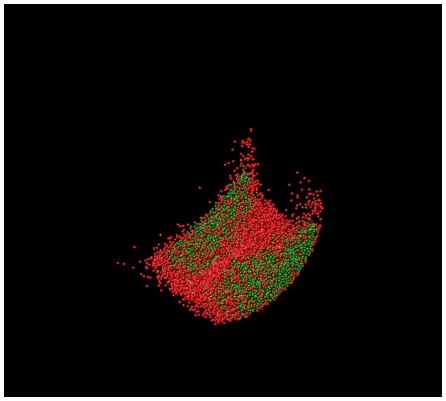

(f) System at $t = 15$ seconds

Figure 3: Simulation of particles inside a rotating cylinder at various points in time. The cylinder is initially stationary, after which it starts rotating at 20 rotations per minute. The green particles have diameter 1.5 times that of the red particles. 20 000 red particles are 6000 green particles were used. The cylinder length was 100 mm and the radius was 65 mm, with the red particle radius being 2 mm.

3 The Experiment

3.1 Experimental Design

This experiment intended to reproduce the effect from the computational simulation carried out by [5], with the aim of investigating why radial segregation happens. In our experiment, the cylinder was half-filled with particles (glass beads), as in the simulation. Two sets of particles were used, with diameters of 3 mm and 5 mm respectively. The particle sizes were decided based upon the sizes used in the paper and the beads that we had access to. We took the same volume of particles for each diameter. We expected some sort of segregation of the particles, and therefore having equal volumes would ensure that the segregated regions were of the same volume. These particles were placed in a cylindrical drum with a diameter of 11.00 ± 0.82 cm. We mixed the particles by shaking the cylinder vigorously in all directions. The expectation was that if the cylinder was shaken vigorously enough and without any bias to any direction, then segregation effects would not occur and this would result in the particles being uniformly mixed.

The cylinder was rotated by means of a rotational rig. It rotated the cylinder at a constant rate of about 100 rotations per minute (rpm). This speed was purely determined by the build of the rig and not set for this experiment in particular.

To determine the global behaviour of the medium we use the Lagrangian specification of the flow field, that is the movement of a single tracer particle, to determine the Eulerian specification of the flow field which considers the flow of the medium at all points in the cylinder simultaneously. The PEPT camera enables us to track the motion of a single irradiated tracer particle accurately by triangulating its position from the emitted back to back gamma rays.

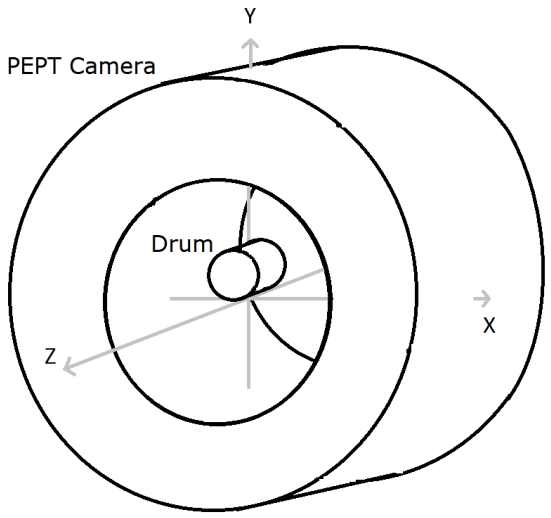

Figure 4: Schematic drawing of the set-up of the experiment, including the coordinate axes. The drum was positioned at the center of the camera.

The tracer particle was created by embedding liquid ^{68}Ga (which has a half-life of 68 minutes) inside a glass bead. A tracer particle of each diameter (3 mm and 5 mm) was used for the experiment, so that the movement of both particles could be analysed. The entire rig was placed in the PEPT camera. This set-up is illustrated in Fig. 4. The measurements we took were around 5 minutes long. We expected this to be more than enough time for the system to reach a steady state. We also took a longer run of around 15 minutes for each particle to check that the behaviour remains consistent.

3.2 Method

3.2.1 Optimisation

We had to perform measurements of the behaviour of the particles in the stationary state, to help determine the degree of attenuation and scattering of the 511 keV gamma rays, which is encoded in an optimisation parameter and used in the triangulation algorithm. To do this, we half-filled the cylinder with the bidisperse mixture of particles and a tracer particle of either diameter. Then we shook the cylinder to ensure that each of the bead sizes were distributed evenly throughout the drum. We then placed the cylinder on the stationery rig and collected measurements from the PEPT camera for 5 minutes.

3.2.2 Measurements

In order to prepare the cylinder, we placed both sets of particles (3 mm and 5 mm) and the tracer inside. The lid was then closed, and the drum was shaken vigorously by hand in all directions until the particles inside were assumed to be evenly distributed throughout the volume. Being very careful not to move the drum more than necessary, the drum was then placed sideways onto the rotational rig. After starting the PEPT camera, the rig was switched on and the motor rotated the drum for 4-5 minutes, after which the data was saved and the cylinder prepared for the next reading. The cylinder was prepared by shaking it again in an attempt to redistribute the particles uniformly. This procedure was then repeated many times for each tracer particle (3 mm and 5 mm, we took 15 of each in total). We also took 15 minute runs for each particle.

3.3 Practical considerations and recommendations

^{68}Ga has a half-life of 68 minutes. This means each experiment had to be designed with consideration to this time constraint. The size of the data also had to be taken into account, as the PEPT camera outputs data at a very fast rate. Therefore, we had to ensure that only necessary measurements were being made and the camera did not run for longer than needed. Large amounts of data are more difficult to transport/share and require more computational power to analyse.

Upon running the rotational rig with the drum, it was found that the drum shifted along the rig as time progressed. This would be problematic, since the movement of particles in the drum would be inaccurately captured by the detectors. It is for this reason that metal stands were fixed into place on both ends of the drum. This led to a non-shifting drum, whilst ensuring that the rotational velocity of the drum was not inhibited in any way.

A possible improvement which can be made to this experiment is to find a better method to uniformly distribute the particles throughout the volume of the drum. The method employed for these measurements involved simply shaking the drum arbitrarily in all directions. While this may be sufficient for most purposes, we cannot certainly say that the particles were uniformly distributed throughout the volume of the drum.

For further research we would recommend using beads of different ratios; a larger disparity in diameters could lead to a more pronounced effect on the system to be analysed. It would also be interesting to vary the speed of rotation and investigate how this might affect the system.

4 Data Analysis

4.1 Optimisation

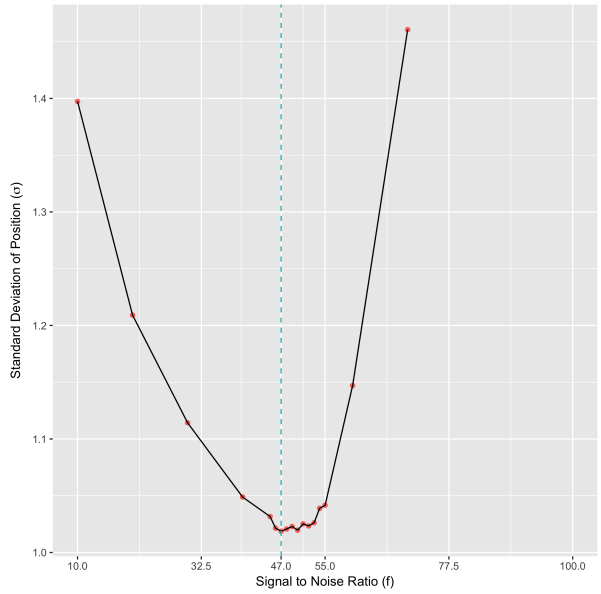

Figure 5: Standard deviation in 3D location, σ, as a function of fraction of trajectories, f. In pink the data points are plotted with a blue dotted line to represent the optimal f - corresponding to the lowest σ at 47.

The raw data from the optimisation file was run through the ctrack algorithm, the fraction of trajectories kept was varied from 10 to 100 in increments of 10 while the other parameters were kept constant as their defaults.

The standard deviation of the locations was calculated for each of the three co-ordinates - σ_x, σ_y and σ_z. Since the algorithm seems to give unbiased locations [8], these were taken to be the uncertainty in location. The 3D standard deviation was then calculated in the following way:

$$\sigma = \sqrt{\sigma_x^2 + \sigma_y^2 + \sigma_z^2}$$

The 3D standard deviation was plotted as a function of the fraction of trajectories - the various chosen f values - to find the optimal f. This was determined by finding the f value that corresponded to the lowest 3D standard deviation. To get a more precise result the process was repeated based on the results of the plot, choosing f values 5 below and 5 above the first found optimal f increasing increments of 1. The 3D standard deviations of these data sets were then overlaid on the previous plot to find a more precise optimal f.

The first plot of the standard deviation in 3D location, σ, as a function of fraction of trajectories, f, found a minimum/optimal f of 50. The next range of data was taken with f from 45 to 55 in increments of 1. The results are plotted in Fig. 5. The optimal f was then found to be 47 and used for all further analysis of the data.

4.2 Frequency Plots

We plotted an XY-position plot of the data, with a colour map indicating the particle frequency (the number of times the particle visited that position) of each position in the data set, for both the 3 mm and 5 mm particles. We attempted to plot this for the full data set (all runs combined), but did not have the computing power to process over 800000 points in a reasonable amount of time. We decided to plot one run for each particle, with 1 mm^2 bins.

We can see from Fig. 6a that particle frequency for the 3 mm particle is greater towards the edge of the rotating bed, and there are few particles towards the centre of rotation. From Fig. 6b we find that the frequency is more evenly spread in this case. Note that both plots have a small area of very high density, representing the initial position of the particle.

As illustrated by the frequency plots shown in Fig.s 6a and 6b, we see that a "core" of larger particles forms at the bottom of the free surface inside the drum, while the smaller particles are found closer to the edges of the drum. This type of segregation occurs at higher rotational speeds than the classic Brazil nut effect, in which smaller particles form a core below the free surface, as discussed in the Theory section.

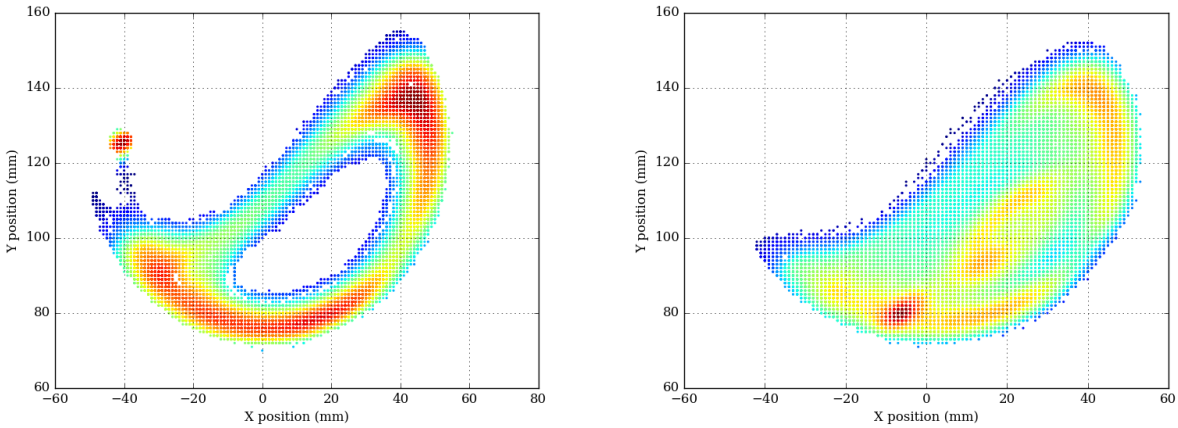

(a) (b)

Figure 6: Frequency scatter plot of XY position, with 1 mm^2 bins, for the 5 mm and 3 mm particles.

4.3 Velocity Vector Fields

Making use of six data sets for each of the two particles sizes, where each data set was calibrated so that the centre of the drum was at the origin, the average vector field for each of the particle sizes was determined. The individual velocity measurements were made by using the 6-point average method [9]:

$$\begin{aligned}\vec{v}_i = 0.1\left[\frac{\vec{P}_{i+5}-\vec{P}_i}{t_{i+5}-t_i}\right] + 0.15\left[\frac{\vec{P}_{i+4}-\vec{P}_{i-1}}{t_{i+4}-t_{i-1}}\right] + 0.25\left[\frac{\vec{P}_{i+3}-\vec{P}_{i-2}}{t_{i+3}-t_{i-2}}\right] \\ +0.25\left[\frac{\vec{P}_{i+2}-\vec{P}_{i-3}}{t_{i+2}-t_{i-3}}\right] + 0.15\left[\frac{\vec{P}_{i+1}-\vec{P}_{i-4}}{t_{i+1}-t_{i-4}}\right] + 0.1\left[\frac{\vec{P}_i-\vec{P}_{i-5}}{t_i-t_{i-5}}\right]\end{aligned} \tag{4.1}$$

The final average velocity fields were determined by taking an average of all the velocity measurements inside 1 mm^2 grid blocks. These fields are shown in Fig. 7.

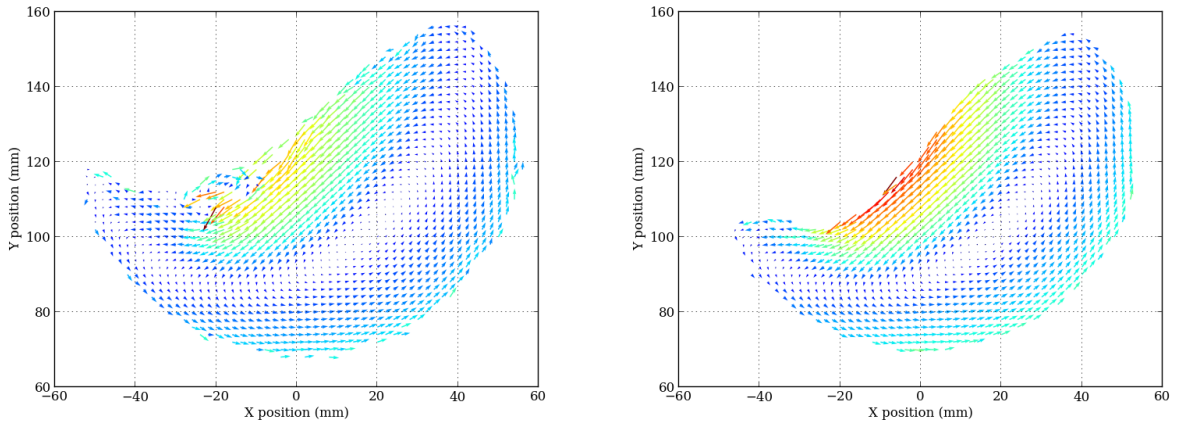

(a) (b)

Figure 7: The average velocity field of (a) the 3 mm particle and (b) the 5 mm particle. The vectors have been scaled arbitrarily, and colour coded by magnitude.

Once the complete average vector fields were determined, we consider the velocity with respect to the "free surface" axis. For each velocity measurement made, the component perpendicular to the free surface (i.e. parallel to the y axis in Fig. 1) was determined, and the average velocity field along that axis was plotted in the same manner as before. The free surface was determined to be at a 45 degree angle to the X axis established by the detector.

Finally, in order to compare these velocities directly, and observe the segregation behaviour expected, the difference between the 3 mm vector components and the 5 mm vector components, at the same points in the drum, were determined. This is illustrated in Fig. 8. The difference is positive along the top of the free surface (and dips down at the left-most edge due to the gravitational and rotational forces), and points down at the bottom of the drum. This is consistent with the density plot observations. The small particle tends to move towards, and along, the outside of the range of motion. On the other hand, the larger particle's velocities have a smaller magnitude towards the edges, which is consistent with the observation that they spend more time in the "core" below the free surface.

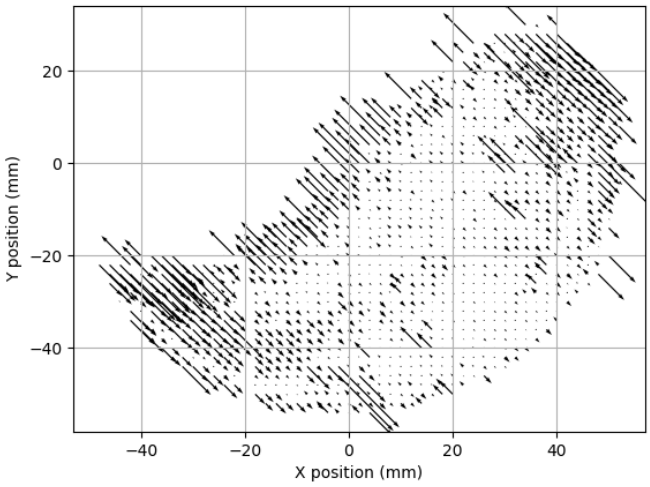

Figure 8: The difference between the average velocity components perpendicular to the free surface for the 3 mm particle and the 5 mm particle. The velocity field of the 5 mm particle was subtracted from the velocity field of the 3 mm particle to get the difference given above. We can see that the small particle has a greater magnitude in velocity towards, and along, the edges of the range of motion.

5 Conclusion

Rather than observing the conventional Brazil nut effect in the free surface, where small particles accrete in the core of the cylinder, we observe that the large particles form the core. This effect is observed when the rotational speed is sufficiently high. No comment could be made about the precise mechanism which causes this type of radial segregation. It seems that radial segregation originates in the free surface. The relative velocity normal to the free surface of the two types of particles results in one type migrating down to the core, where there is less movement of the particles. We carried out rudimentary uncertainty analysis in obtaining the results, however to definitively support this conclusion more precise uncertainty analysis would have to be carried out.

For further research we recommend considering the effect of varying the rotational speed. Much of the literature concerning radial segregation in the continuous flow regime reports a core of small particles forming. In this analysis the rotational speed was sufficiently high to observe a core of large particles forming. It might be insightful to investigate the rotational speed at which the behaviour transitions.

Appendices

A A Mathematical Model of Radial Segregation

In this section, we consider a mathematical model that describes the occurrence of segregation in a rotating drum containing two types of granular material. This model was obtained from [10] and the discussion therein will be closely followed below.

We begin by considering a rotating cylindrical drum containing two types of particles. The drum has a radius R and is rotating at an angular frequency ω. For simplicity, we shall suppose that both particles are identical rigid spheres, differing only in radius. That is, we are considering a partially filled, rotating drum containing large particles B as well as small particles S. In describing this system, we make the assumption that the surface profile of the granular system remains unchanged as the drum rotates. We shall align our x-axis such that it passes through the centre of the drum as well as the two points of contact between the surface profile and the drum walls. Furthermore, we align our y-axis along the axial direction of the drum.

In order to construct a mathematical model of this system, it is prudent to consider the relative concentrations of the two types of particles. By considering the number density of the small particles $\phi = \phi(t, \mathbf{r})$, it is possible to introduce the concentration field $\psi = \psi(t, \mathbf{r})$ as

$$\psi = 2\phi - 1, \tag{A.1}$$

where $-1 \leq \psi \leq 1$. We interpret ψ as a field that describes the relative concentration of the two types of particles. Furthermore, we impose the condition that if $\psi < 0$ in a region, then the region has a greater concentration of large particles and if $\psi > 0$ in a region, then the region has a greater concentration of small particles. To this end, if $\psi = -1$ in a region, then that region contains only large particles. Analogously, if $\psi = 1$ in a region, then that region contains only small particles.

Our goal is to derive a time-evolution equation for the concentration field, ψ. In order to do this, we must consider the types of currents that occur in the rotating drum. We consider first the current term describing the motion down the surface of the granular media. This term can be written as

$$\mathbf{j}_1 = m_0(1 - \psi^2)\nabla(s(x) - s_B(x)), \tag{A.2}$$

where $s(x)$ is the slope function of the system and $s_B(x)$ is the slope function of a system containing only large particles. m_0 is the mobility of the particles and is proportional to the angular frequency ω of the rotating drum.

If a region that contains a high concentration of small particles interacts with a region that contains a high concentration of large particles, there will be little exchange of particles. This phenomenon gives rise to the following current:

$$\mathbf{j}_2 = Q(1 - \psi^2)\nabla(\nabla^2\psi) \ , \tag{A.3}$$

where Q is a constant proportional to the angular frequency of the rotating drum. Thus the time-evolution equation can be written as follows:

$$\frac{\partial \psi}{\partial t} = D\nabla^2\psi - \nabla\cdot\mathbf{j}_t, \tag{A.4}$$

where $\mathbf{j}_t \equiv \mathbf{j}_1 + \mathbf{j}_2$ is the total current of the system and D is a constant proportional to the angular frequency of the rotating drum. In the case where the drum is not rotating, we have $Q = m_0 = D = 0$ and so, from equation (A.4), ψ remains constant, as expected.

In order to find an explicit form for $\mathbf{j}_t$, it is necessary to determine an expression for $s(x) - s_B(x)$ - the difference of the slope functions. To find such an expression, we begin by determining an expression for

$s_B(x)$. To this end, consider a rotating drum containing only large particles. Here, at the walls of the container, the slope function $s_B(x)$ should depend only on the coefficient of friction μ_B. In addition, in the case where $\omega = 0$, the slope function should depend only on the coefficient of friction *everywhere*. It follows that the most general form that the slope function can take is that of the following [10]:

$$s_B(x) = \mu_B + \sum_{n=0}^{\infty} f_n(\omega)(R^2 - x^2)^n, \tag{A.5}$$

where $f_n(0) = 0$ so as to ensure that $s_B(x)$ depends only on μ_B in the case where $\omega = 0$. We may Taylor expand the $f_n(\omega)$ terms:

$$f_n(\omega) \approx f_n(0) + \omega f_n'(0) = \omega f_n'(0) \ .$$

By letting $g_n = f_n'(0)$, equation (A.5) becomes

$$s_B(x) = \mu_B + \sum_{n=0}^{\infty} \omega g_n(R^2 - x^2)^n \ . \tag{A.6}$$

Therefore, if we regard μ and g_n as functions of ψ, the slope function of the two particle system can be written as

$$s(x) = \mu(\psi) + \sum_{n=0}^{\infty} \omega g_n(\psi)(R^2 - x^2)^n. \tag{A.7}$$

We write g_n as a power series in ψ and obtain

$$g_n(\psi) = \sum_{k=0}^{\infty} b_{n,k}\psi^k, \tag{A.8}$$

where $b_{n,k}$ is a constant. In the case of s_B, we take $\psi = -1$. Therefore, the difference of the two slope functions is

$$s(x) - s_B(x) = \mu + \mu_B + \sum_{n=0}^{\infty}\sum_{k=0}^{\infty} \omega(\psi^k b_{n,k} - c_{n,k}(-1)^k)(R^2 - x^2)^n. \tag{A.9}$$

It follows that equation (A.4) becomes

$$\frac{\partial \psi}{\partial t} = D\nabla^2\psi - \nabla\cdot\left[(1-\psi^2)\nabla(m_0(\mu + \mu_B + \sum_{n=0}^{\infty}\sum_{k=0}^{\infty} \omega(\psi^k b_{n,k} - c_{n,k}(-1)^k)(R^2 - x^2)^n) + Q\nabla^2\psi)\right]. \tag{A.10}$$

We would now like to determine an expression for ψ by making use of equation (A.10) and by considering only radial segregation. To do this, consider the case where the system has reached a state of equilibrium and thus $\frac{\partial \psi}{\partial t} = 0$. Furthermore, since we are only interested in radial segregation, we consider a concentration field $\psi = \psi(x)$ that depends only on x.

We set $\frac{\partial \psi}{\partial t} = 0$ in equation (A.10) and, after neglecting higher order terms and small contributions to this sum, we obtain

$$D\frac{\partial^2 \psi}{\partial x^2} = \frac{\partial}{\partial x}\Big\{m_0(1-\psi^2)\frac{\partial}{\partial x}(a\omega(R^2 - x^2))\Big\}, \tag{A.11}$$

where a is a constant and $m_0, D > 0$ since $\omega > 0$. By solving the above equation, we obtain

$$\left|\frac{\psi + 1}{\psi - 1}\right| = Ae^{-\frac{2m_0 a\omega x^2}{D}}, \tag{A.12}$$

where $A > 0$ is a constant. Since we have $-1 \leq \psi \leq 1$, it follows that equation (A.12) becomes

$$\frac{\psi + 1}{\psi - 1} = -Ae^{-\frac{2m_0 a\omega x^2}{D}}, \tag{A.13}$$

and thus,

$$\boxed{\psi = \frac{Ae^{-\frac{2m_0 a\omega x^2}{D}} - 1}{Ae^{-\frac{2m_0 a\omega x^2}{D}} + 1}}. \tag{A.14}$$

By making use of equation (A.14), it is possible to produce a plot of ψ vs x. Such a plot is shown in Fig. 9.

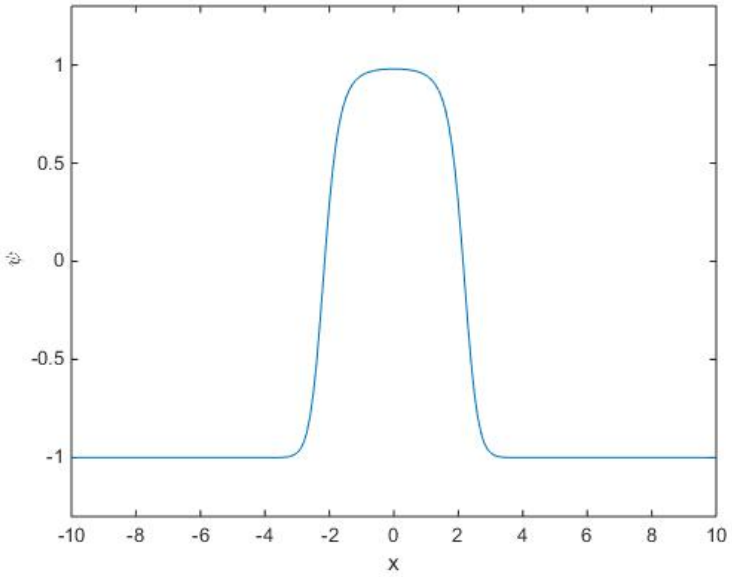

Figure 9: The plot shown here depicts how the relative concentration of the media, ψ, changes as a function of x. In order to produce this plot, equation (A.14) was used with the constants set to: $A = 100$ and $\frac{2m_0 a\omega}{D} = 1$. The plot shows that the small particles collect in the centre of the drum and the larger ones are pushed to the edges.

From Fig. 9 it can be noticed that, for $a > 0$, as the distance from the centre of the drum increases in magnitude along the x-axis, the value of ψ decreases. Therefore, it is expected that, at the centre of the drum, we are more likely to find regions that have a higher concentration of small particles. Similarly, we expect to find the regions near the sides of the drum to have a higher concentration of large particles.

Furthermore, it can be noticed that if we were to instead consider $a < 0$ in this model, the opposite effect would occur and we would have central regions containing a higher concentration of large particles and the outer regions containing a higher concentration of small particles.

B Computational

The set up for the granular material simulations in the Computation section is as follows. Each particle was represented as a rigid sphere of given radius r and mass m. Two types of particles were used for our simulations, where the particle with larger radius is drawn in green, whereas the particle with smaller radius is drawn in red. We assumed both particles had the same density.

Each particle was subject to the force of gravity in the $-\hat{\mathbf{z}}$ direction, a pairwise interaction force and a normal and frictional force with the rotating cylinder whenever the particle was in contact with the cylinder.

The pairwise interaction used for the simulation was a Hertzian style interaction [6], as described in [4, 11, 12]. To calculate the frictional force between two particles i and j, we denote the radius of particle i as R_i and the radius of particle j as R_j with their contact distance being $d = R_i + R_j$. If the particles are a distance r away from each other, we calculate the frictional force between the two particles as:

$$\mathbf{F} = \begin{cases} \sqrt{\delta}\sqrt{\frac{R_i R_j}{R_i + R_j}}\mathbf{F}_{hooke} & \text{if } r < d \\ 0 & \text{if } r > d \end{cases} \tag{B.1}$$

where $\mathbf{F}_{hooke}$ is given as

$$\mathbf{F}_{hooke} = \mathbf{F}_n + \mathbf{F}_t = (k_n \delta \mathbf{n}_{ij} - m_{\text{eff}} \gamma_n \mathbf{v}_n) - (k_t \Delta \mathbf{s}_t + m_{\text{eff}} \gamma_t \mathbf{v}_t) \tag{B.2}$$

where $\delta = d - r$ denotes the overlap distance between particles i and j. The first bracket in equation (B.2) denotes the *normal* component $\mathbf{F}_n$ of the force whereas the second bracket denotes the *tangential* component $\mathbf{F}_t$. The relevant quantities given in equation (B.2) are described below.

k_n, k_t is the elastic constant for normal and tangential contact respectively, γ_n, γ_t is the visco-elastic damping constant for normal and tangential contact respectively, $m_{\text{eff}} = (M_i M_j)/(M_i + M_j)$ is the effective mass of the two particles, $\Delta \mathbf{s}_t$ is the tangential displacement vector between the two particles, $\mathbf{n}_{ij}$ is the unit vector along the line connecting the centres of the two particles and $\mathbf{v}_n$, $\mathbf{v}_t$ is the normal and tangential component of the relative velocity of the two particles respectively.

Values for k_n and k_t were calculated as:

$$k_n = \frac{4G}{3(1-\nu)} \quad \text{and} \quad k_t = \frac{4G}{2-\nu} \tag{B.3}$$

as done in [12] where $\nu = \frac{2}{7}$ denotes the Poisson ratio used in the simulation. G, the shear modulus, can be calculated as:

$$G = \frac{E}{2(1+\nu)} \tag{B.4}$$

where E is Young's modulus. A value of $E = 10^5$ N m^{-2} was used for all simulations.

We also note a coefficient of friction μ which gives an upper limit to the tangential force $F_t \leq \mu F_n$. A value of $\mu = 0.5$ was used for all simulations.

References

[1] M. Nakagawa, S.A. Altobelli, A. Caprihan, E. Fukushima, and E.K. Jeong. "Non-invasive measurements of granular flows by magnetic resonance imaging". In: *Experiments in Fluids* 16 (1993), pp. 54–60.

[2] F. Catelaube and D. Bideau. "Radial Segragation in a 2d Drum: An Experimental Analysis". In: *Europhys. Lett.* 30 (3 1995), pp. 133–138.

[3] N. Brodu, J.A. Dijksman and R.P. Behringer. "Spanning the scales of granular materials through microscopic force imaging". In: *Nature communications* 6 (2015).

[4] N.V. Brilliantov, F. Spahn, J. Hertzsch and T. Pöschel. "Model for collisions in granular gases". In: *Phys. Rev. E* 53.5 (1996), pp. 53–82.

[5] G. Baumann, I.M. Janosi, and D.E. Wolf. "Particle Trajectories and Segregation in a Two-Dimensional Rotating Drum". In: *Europhys. Lett.* 27 (3 1994), pp. 203–208.

[6] LAMMPS. *Molecular Dynamics Simulator*. URL: `http://lammps.sandia.gov/`.

[7] J.M. Ottino and D.V. Khakhar. "Mixing and Segregation of Granular Materials". In: *Annual Review of Fluid Mechanics* 32 (1 2000), pp. 55–91.

[8] D.J. Parker. "Positron emission particle tracking - a technique for studying flow with engineering equipment". In: *Nuclear Instruments and Methods in Physics Research* 596 (2005).

[9] T. W. Leadbeater, D. J. Parker and J. Gargiuli. "Positron imaging systems for studying particulate, granular and multiphase flows". In: *Particuology* 10 (2012), pp. 146–153.

[10] S. Puri and H. Hayakawa. "Segregation of Granular Mixtures in a Rotating Drum". In: (1999). URL: `https://arxiv.org/abs/cond-mat/9901260v1)`.

[11] L.E. Silbert et al. "Granular flow down an inclined plane: Bagnold scaling and rheology". In: *Phys. Rev. E* 64 (5 2001), p. 051302.

[12] H.P. Zhang and H.A. Makse. "Jamming transition in emulsions and granular materials". In: *Physical Review E* 72.1 (2005), p. 011301.